

Molecules in high spin states III: The millimeter/submillimeter-wave spectrum of the MnCl radical ($X\ 7\ \Sigma^+$)

D. T. Halfen and L. M. Ziurys

Citation: *The Journal of Chemical Physics* **122**, 054309 (2005); doi: 10.1063/1.1824036

View online: <http://dx.doi.org/10.1063/1.1824036>

View Table of Contents: <http://scitation.aip.org/content/aip/journal/jcp/122/5?ver=pdfcov>

Published by the [AIP Publishing](#)

Articles you may be interested in

[Fine structure and hyperfine perturbations in the pure rotational spectrum of the VCl radical in its \$X\ \Delta\ 5\ r\$ state](#)
J. Chem. Phys. **130**, 164301 (2009); 10.1063/1.3108538

[Perturbations in the pure rotational spectrum of CoCl \(\$X\ 3\ \Phi\ i\$ \): A submillimeter study](#)
J. Chem. Phys. **121**, 8385 (2004); 10.1063/1.1795691

[Fourier transform microwave spectroscopy and Fourier transform microwave–millimeter wave double resonance spectroscopy of the ClOO radical](#)
J. Chem. Phys. **121**, 8351 (2004); 10.1063/1.1792591

[Molecules in high spin states: The millimeter and submillimeter spectrum of the MnS radical \(\$X\ 6\ \Sigma^+\$ \)](#)
J. Chem. Phys. **116**, 10212 (2002); 10.1063/1.1476931

[Millimeter-wave spectroscopy of FeF \(\$X\ 6\ \Delta\ i\$ \): Rotational analysis and bonding study](#)
J. Chem. Phys. **106**, 3494 (1997); 10.1063/1.473446



Molecules in high spin states III: The millimeter/submillimeter-wave spectrum of the MnCl radical ($X^7\Sigma^+$)

D. T. Halfen and L. M. Ziurys^{a)}

Department of Chemistry, Department of Astronomy, Arizona Radio Observatory, and Steward Observatory, University of Arizona, Tucson, Arizona 85721

(Received 3 August 2004; accepted 4 October 2004; published online 18 January 2005)

The pure rotational spectrum of the MnCl radical ($X^7\Sigma^+$) has been recorded in the range 141–535 GHz using millimeter–submillimeter direct absorption spectroscopy. This work is the first time the molecule has been studied with rotational resolution in its ground electronic state. MnCl was synthesized by the reaction of manganese vapor, produced in a Broida-type oven, with Cl_2 . Transitions of both chlorine isotopomers were measured, as well as lines originating in several vibrationally excited states. The presence of several spin components and manganese hyperfine interactions resulted in quite complex spectra, consisting of multiple blended features. Because 42 rotational transitions were measured for Mn^{35}Cl over a wide range of frequencies with high signal-to-noise, a very accurate set of rotational, fine structure, and hyperfine constants could be determined with the aid of spectral simulations. Spectroscopic constants were also determined for Mn^{37}Cl and several vibrationally excited states. The values of the spin-rotation and spin–spin parameters were found to be relatively small ($\gamma=11.2658$ MHz and $\lambda=1113.10$ MHz for Mn^{35}Cl); in the case of λ , excited electronic states contributing to the second-order spin–orbit interaction may be canceling each other. The Fermi contact hyperfine term was found to be large in manganese chloride with $b_F(\text{Mn}^{35}\text{Cl})=397.71$ MHz, a result of the manganese $4s$ character mixing into the 12σ orbital. This orbital is $sp\sigma$ hybridized, and contains some Mn $4p\sigma$ character, as well. Hence, it also contributes to the dipolar constant c , which is small and positive for this radical ($c=32.35$ MHz for Mn^{35}Cl). The hyperfine parameters in MnCl are similar to those of MnH and MnF, suggesting that the bonding in these three molecules is comparable. © 2005 American Institute of Physics. [DOI: 10.1063/1.1824036]

I. INTRODUCTION

Of all the $3d$ transition metals, manganese-bearing molecules are likely to exhibit some of the most complex spectra. The electron configuration of this atom is $4s^23d^5$, i.e., a half-filled $3d$ shell. Hence, resulting electronic states for even diatomic species are high-spin; MnH and the manganese halides, for example, have $^7\Sigma^+$ ground states,^{1–3} while MnO and MnS exhibit $^6\Sigma^+$ ground-state terms.^{4,5} No theoretical or experimental work exists for MnC, but in the case of MnN, there are density functional theory (DFT) calculations, which suggest the molecule is a quintet in its ground state.⁶ The ^{55}Mn nucleus has a spin of $I=5/2$ as well, and given the presence of multiple unpaired electrons in these species, complicated hyperfine structure can result. In fact, in both MnH and MnF, the hyperfine coupling is sufficiently strong that it competes with the spin interactions, inducing rotationally forbidden $\Delta J=\pm 2$ and ± 3 transitions.^{2,7}

Another manganese molecule of interest is MnCl. The first laboratory observation of this species occurred over 60 years ago by Mesnage and Bacher, who studied the ultraviolet spectrum of the $A^7\Pi-X^7\Sigma^+$ and $B^7\Sigma^+-X^7\Sigma^+$ transitions, respectively.^{3,8} Later work on the visible and ultraviolet spectrum of MnCl established vibrational parameters for the $A^7\Pi-X^7\Sigma^+$ transition and two bands in the blue–green

region using classical hollow cathode emission techniques.^{9,10} More recently, the $c^5\Sigma^+-a^5\Sigma^+$ band in the infrared was rotationally resolved using Fourier transform emission spectroscopy, and vibrational, rotational, and fine structure constants were obtained for both states.¹¹ In addition, an electron spin resonance (ESR) study of manganese chloride in an argon matrix by Baumann, Van Zee, and Welner established estimates of the manganese hyperfine parameters for the first time.¹² Thus far, however, a rotational analysis for the ground $X^7\Sigma^+$ state has not been conducted. There are also no theoretical estimates of the rotational parameters.

In this paper, we present the first study of MnCl with rotational resolution in its $X^7\Sigma^+$ state. A very large data set extending over 42 transitions of the main isotopic species, Mn^{35}Cl , in its ground vibrational state, has been obtained along with more limited measurements of the $v=1$ and 2 vibrational states. Spectra of the Mn^{37}Cl isotopomer have been recorded as well in its $v=0$ and 1 states. The spectra display a complicated pattern of hypermultiplets that evolve over a range of rotational transitions. These data have been modeled using a Hund's case (b) basis and spectroscopic parameters have been determined. Interpretation of the fine and hyperfine constants in comparison with those of other Mn-bearing molecules has also been carried out. Here we present our data and results.

^{a)}Electronic mail: lziurys@as.arizona.edu

II. EXPERIMENT

The spectra of MnCl were recorded using the high-temperature millimeter–submillimeter-wave direct absorption spectrometer of the Ziurys group, whose basic design is described elsewhere.¹³ Briefly, the instrument consists of a radiation source (Gunn oscillators/Schottky diode multipliers) covering a range of 65–650 GHz, a free-space gas cell containing a Broida-type oven, and a helium-cooled InSb detector. The radiation is propagated through the system by a scalar feedhorn, polarizing grid, offset ellipsoidal mirrors, and a rooftop reflector at the end of the gas cell. A pathlength modulator is employed for baseline smoothing, and the system is under computer control. The radiation is FM modulated and the signals are detected at $2f$ to give a second derivative spectrum.

MnCl was synthesized by the reaction of manganese vapor, produced in the Broida oven, with 1–3 mTorr of Cl_2 . The chlorine gas was added through a tube located over the top of the oven, while ~ 10 mTorr of argon carrier gas was also flowed from under the oven to entrain the metal vapor. To vaporize manganese, the oven power supply required 770 W, and the heating chamber of the oven was insulated with ceramic spheres, alumina fragments, and zirconia felt. No DC discharge was required to produce signals, suggesting that the reaction conditions to create MnCl were quite favorable. Chemiluminescence was not observed during the reaction.

As described in the next section, initially a wide frequency range (~ 21 GHz) had to be searched in 100 MHz sections to locate the various vibrational states of MnCl and establish harmonic relationships. Once the rotational constants were determined, frequencies of other transitions could be very accurately predicted such that little additional scanning was needed. Precise rest frequencies of individual transitions were determined by averaging pairs of 6 MHz wide scans, one increasing and the other decreasing in frequency. Typically only 1 to 2 such pairs were needed for strong lines but 3 to 4 pairs were necessary for the higher vibrational states. Gaussian fits to the observed line profiles were used to determine the center frequency and line width, which ranged from 500 kHz at 141 GHz to 1400 kHz at 535 GHz for unblended lines. The experimental error is estimated to be ± 50 kHz.

III. RESULTS

Because no previous high resolution data was available for the $^7\Sigma^+$ ground state of MnCl, a rotational constant was estimated assuming a bond length of 2.23 Å—slightly longer than that of CrCl and FeCl. A range of 21 GHz (~ 4.5 B) was then continuously scanned (450–471 GHz). In this process, various sets of harmonically related multiplets were found, some with very strong signals. These multiplets, however, were not simple septets, as might be expected for a molecule with a $^7\Sigma^+$ ground state. Rather, they had two strong outer features with multiple irregularly spaced and blended lines in between, typically covering a total of 60 MHz in frequency (see Fig. 1). Creation of these features required the presence of both Mn vapor and chlorine gas. A vibrational sequence

could be identified in the strongest lines from $v=0$ to $v=4$. This pattern, including the vibrational series up to $v=2$, was duplicated in a weaker sequence about a factor of three less in intensity. These patterns had to arise from the two chlorine isotopomers of MnCl.

The irregular multiplets are a result of competition between the fine and hyperfine structure interactions. Both manganese and chlorine have nuclear spins of $I(\text{Mn})=5/2$ and $I(\text{Cl})=3/2$. A combination of fine and hyperfine interactions could potentially generate $(2S+1)(2I_1+1)(2I_2+1)=168$ lines per transition $N \rightarrow N+1$. However, the magnetic moments of both chlorine isotopes are over a factor of four less than that of manganese [$\mu_I(\text{Mn})=3.461 \mu_N$ vs $\mu_I(^{35}\text{Cl})=0.82086 \mu_N$ and $\mu_I(^{37}\text{Cl})=0.6833 \mu_N$].¹⁴ Furthermore, the unpaired electrons are most likely to be centered on the Mn atom, as has been found in MnF_2 .² In fact, in manganese fluoride, the ^{19}F nucleus contributed very little to the hyperfine structure, although its magnetic moment is $2.62728 \mu_N$ —over a factor of three greater than those of the chlorine isotopes.¹⁴ Hence, in MnCl, only the manganese spin must be considered, generating at most 42 components per transition. Because the fine and hyperfine structures in MnCl have comparable splittings, 42 individual lines were never resolved in the spectra, even at the lower N values, where these interactions should be largest.

In order to evaluate these complicated patterns, 42 transitions of the main isotopomer, $\text{Mn}^{35}\text{Cl}(v=0)$, were recorded over a broad frequency range (141–535 GHz). A subset of these transitions is given in Table I. (For the complete data set, see EPAPS.¹⁵) The $N=16 \rightarrow 17$ transition was one of the lowest studied in frequency. In this case, a total of 30 individual features were resolved, as shown in the table. Some of these lines are blends of several hyperfine components. The blending increased with frequency, such that at the higher transitions, for example, $N=49 \rightarrow 50$, only 15 individual features could be distinguished (see Table I).

In addition to the $v=0$ state of Mn^{35}Cl , five transitions in each of the $v=1$ and $v=2$ states were measured, along with seven and four transitions of Mn^{37}Cl in its $v=0$ and $v=1$ states, respectively. Selected transitions of these data sets are given in Table II. The complete data set is available from EPAPS.¹⁵ Overall, 1200 individual features were measured, which contribute to 2646 transitions.

The complexity of the MnCl spectra is illustrated in Fig. 1, which shows the $N=16 \rightarrow 17$, $N=34 \rightarrow 35$, and $N=49 \rightarrow 50$ rotational transitions of the main isotopomer near 161, 330, and 470 GHz, respectively, in the ground vibrational state. These data illustrate the competition between the fine and hyperfine interactions. For the highest frequency transition (bottom panel), at least some of the seven spin components, indicated by F_1, F_2, \dots, F_7 , can be individually identified because the hyperfine structure is collapsed. (F_1 corresponds to $J=N+3$, F_2 is $J=N+2$, etc.) For the intermediate frequency transition (middle panel), the extent of the hyperfine interactions has increased such that only the two outer spin components (F_1 and F_7) are clearly distinguishable. These features now appear to exhibit some hyperfine structure as well. In the lowest frequency spectrum (top panel), the hyperfine splitting has become sufficiently large

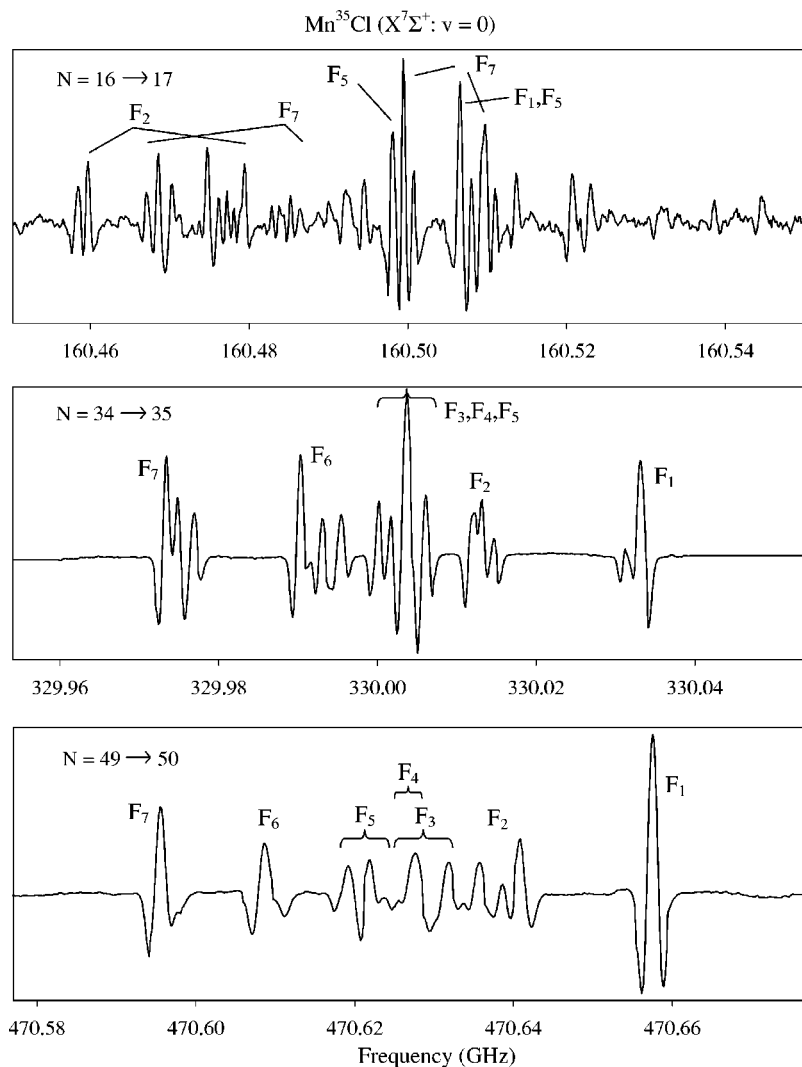


FIG. 1. Spectrum of the $N=16 \rightarrow 17$, $N=34 \rightarrow 35$, and $N=49 \rightarrow 50$ transitions of Mn^{35}Cl ($v=0$) near 161, 330, and 470 GHz, respectively, observed in this work, showing the evolution of the fine–hyperfine interactions. For the $N=49 \rightarrow 50$ transition (bottom panel), the fine structure components on the extrema (F_1 , F_2 , F_6 , and F_7) show little evidence of hyperfine splittings, while the F_3 , F_4 , and F_5 features are partially split and blended together. Increased hyperfine splitting is seen in the $N=34 \rightarrow 35$ spectrum (middle panel), and the inner fine structure components (F_3 , F_4 , and F_5) are no longer distinguishable. The fine and hyperfine structures are totally interspersed for the $N=16 \rightarrow 17$ transition (top panel), such that assignment of the individual spin components is problematic. Some of the lines are labeled to illustrate this effect. Each spectrum is a single scan, 100 MHz in frequency coverage, with a duration of about 1 min.

such that the seven fine structure components are not distinguishable. Hyperfine transitions corresponding to what was the center spin components (F_2, F_3, F_4) now appear at the outer edges of the pattern, while the F_1 and F_7 lines are found near the center. These data are further complicated because of the second derivative line profiles, which can produce “ghost” lines. The data for the excited vibrational states of Mn^{35}Cl and for Mn^{37}Cl ($v=0$ and 1) are very similar in appearance.

IV. ANALYSIS

The MnCl data were fit with an effective Hamiltonian consisting of rotational, spin-rotation, spin–spin, and magnetic hyperfine interactions

$$\hat{H}_{\text{eff}} = \hat{H}_{\text{rot}} + \hat{H}_{\text{sr}} + \hat{H}_{\text{ss}} + \hat{H}_{\text{hf}}. \quad (1)$$

The Hamiltonian was incorporated into SPFIT, a nonlinear least-squares analysis routine developed by Pickett.¹⁶ The code was adapted such that higher-order spin and hyperfine parameters (γ_s and b_s , for example) could be accommodated in the fit.

To analyze the data, the centers of the hypermultiplets of Mn^{35}Cl and Mn^{37}Cl were fit to an initial B and D for each

vibrational state. After that, significant simulations had to be carried out to determine the fine and hyperfine constants. Mn^{35}Cl ($v=0$) spectra were initially analyzed and the resulting procedure used as a template. The higher frequency (400–535 GHz) transitions were first considered. To fit these data, the values of the fine structure parameters γ and λ of MnF were initially used,² as well as the hyperfine constants b_F and c of MnCl determined from the ESR studies.¹² These parameters were then adjusted to fit the outer spin components ($J=N-3$, $N-2$, $N+2$, and $N+3$, or F_7 , F_6 , F_2 , and F_1), where the fine structure was better resolved, using simulated spectra. The centrifugal distortion corrections to γ , λ , and b_F were added as required. The inner components were then included in the fit. After the higher frequency transitions were successfully reproduced and a set of spectroscopic parameters obtained, the next set of lower frequency transitions (300–400 GHz) were then added to the analysis, followed by the 141–300 GHz set. Many iterations were required to successfully and consistently reproduce the spectra of the entire data set. The $v=1$ and 2 data of the main isotopomer and the $v=0$ and $v=1$ spectra of Mn^{37}Cl were analyzed in an identical manner. These measurements were somewhat easier to fit as they did not include as wide a range in frequency.

TABLE I. Selected rotational transitions of Mn^{35}Cl ($X^7\Sigma^+; v=0$).^a

N''	J''	F''	\rightarrow	N'	J'	F'	ν_{obs}	$\nu_{\text{obs}} - \nu_{\text{calc}}$	N''	J''	F''	\rightarrow	N'	J'	F'	ν_{obs}	$\nu_{\text{obs}} - \nu_{\text{calc}}$
16	17	19.5		17	18	20.5	160 458.362	0.080	34	32	32.5		35	33	33.5	329 990.328	-0.316
16	18	20.5		17	19	21.5	160 459.679	0.005	34	32	31.5		35	33	32.5	329 991.600	0.085
16	13	13.5		17	14	14.5	160 467.183	-0.133	34	32	30.5		35	33	31.5	329 993.089	0.069
16	13	12.5		17	14	13.5	160 468.544	0.087	34	32	29.5		35	33	30.5	329 995.427	-0.030
16	18	19.5		17	19	20.5	160 468.544	-0.106	34	33	35.5		35	34	36.5	330 000.172	0.243
16	13	14.5		17	14	15.5	160 470.238	0.171	34	33	34.5		35	34	35.5	330 000.172	-0.317
16	17	18.5		17	18	19.5	160 470.238	-0.306	34	33	33.5		35	34	34.5	330 001.740	0.321
16	13	11.5		17	14	12.5	160 474.707	0.315	34	33	31.5		35	34	32.5	330 001.740	0.068
16	18	18.5		17	19	19.5	160 474.707	-0.102	34	35	36.5		35	36	37.5	330 001.740	-0.474
16	13	15.5		17	14	16.5	160 476.132	0.104	34	34	35.5		35	35	36.5	330 003.747	0.942
16	16	18.5		17	17	19.5	160 477.252	0.021	34	33	32.5		35	34	33.5	330 003.747	0.812
16	18	15.5		17	19	16.5	160 478.099	0.803	34	34	36.5		35	35	37.5	330 003.747	0.583
16	18	16.5		17	19	17.5	160 478.837	0.001	34	35	37.5		35	36	38.5	330 003.747	0.157
16	18	17.5		17	19	18.5	160 479.425	-0.089	34	33	30.5		35	34	31.5	330 003.747	0.029
16	16	17.5		17	17	18.5	160 483.811	0.498	34	35	35.5		35	36	36.5	330 003.747	-0.026
16	17	17.5		17	18	18.5	160 484.382	-0.444	34	34	34.5		35	35	35.5	330 003.747	-0.174
16	13	10.5		17	14	11.5	160 486.238	-0.057	34	35	34.5		35	36	35.5	330 003.747	-0.419
16	17	16.5		17	18	17.5	160 492.487	0.215	34	35	32.5		35	36	33.5	330 003.747	-0.544
16	16	16.5		17	17	17.5	160 496.455 ^b		49	46	46.5		50	47	47.5	470 595.397	0.173
16	15	14.5		17	16	15.5	160 498.138	0.191	49	46	47.5		50	47	48.5	470 595.397	0.138
16	15	17.5		17	16	18.5	160 498.138	-0.544	49	46	45.5		50	47	46.5	470 595.397	-0.099
16	17	15.5		17	18	16.5	160 499.414	-0.033	49	46	48.5		50	47	49.5	470 595.397	-0.173
16	15	15.5		17	16	16.5	160 499.414	-0.058	49	46	44.5		50	47	45.5	470 595.397	-0.719
16	15	16.5		17	16	17.5	160 499.414	-0.108	49	46	43.5		50	47	44.5	470 597.452	0.312
16	19	21.5		17	20	22.5	160 500.719	-0.015	49	47	49.5		50	48	50.5	470 608.416	0.611
16	17	14.5		17	18	15.5	160 506.530	0.112	49	47	48.5		50	48	49.5	470 608.416	0.228
16	19	16.5		17	20	17.5	160 506.530	0.071	49	47	47.5		50	48	48.5	470 608.416	-0.144
16	19	20.5		17	20	21.5	160 506.530	-0.007	49	47	46.5		50	48	47.5	470 608.416	-0.549
16	14	15.5		17	15	16.5	160 508.033	0.090	49	47	45.5		50	48	46.5	470 609.502	0.020
16	14	14.5		17	15	15.5	160 509.224	0.040	49	47	44.5		50	48	45.5	470 609.502	-0.772
16	14	16.5		17	15	17.5	160 509.224	0.016	49	48	45.5		50	49	46.5	470 619.083	0.418
16	16	15.5		17	17	16.5	160 509.224	-0.092	49	48	46.5		50	49	47.5	470 619.083	-0.453
16	19	17.5		17	20	18.5	160 509.816	0.089	49	48	49.5		50	49	50.5	470 621.768	0.342
16	19	19.5		17	20	20.5	160 509.816	-0.066	49	48	48.5		50	49	49.5	470 621.768	-0.262
16	19	18.5		17	20	19.5	160 510.929	0.025	49	48	50.5		50	49	51.5	470 621.768	-0.436
16	14	13.5		17	15	14.5	160 513.624	-0.193	49	49	46.5		50	50	47.5	470 623.630	0.146
16	15	13.5		17	16	14.5	160 520.636	-0.108	49	48	47.5		50	49	48.5	470 623.630	-0.066
16	16	14.5		17	17	15.5	160 520.636	-0.756	49	49	47.5		50	50	48.5	470 625.571	0.487
16	14	12.5		17	15	13.5	160 522.927	-0.193	49	50	47.5		50	51	48.5	470 625.571	0.373
16	16	13.5		17	17	14.5	160 532.049	-0.126	49	49	48.5		50	50	49.5	470 625.571	-0.343
16	14	11.5		17	15	12.5	160 538.468	-0.062	49	50	48.5		50	51	49.5	470 626.729	0.388
16	15	12.5		17	16	13.5	160 545.088	0.290	49	49	49.5		50	50	50.5	470 626.729	0.202
34	35	33.5		35	36	34.5	330 003.747	-0.661	49	50	49.5		50	51	50.5	470 627.691	0.608
34	34	33.5		35	35	34.5	330 006.019	0.897	49	49	50.5		50	50	51.5	470 627.691	0.458
34	34	32.5		35	35	33.5	330 006.019	-0.045	49	50	50.5		50	51	51.5	470 627.691	0.043
34	34	31.5		35	35	32.5	330 006.019	-0.204	49	49	51.5		50	50	52.5	470 627.691	-0.205
34	36	38.5		35	37	39.5	330 011.652	-0.462	49	50	51.5		50	51	52.5	470 627.691	-0.753
34	36	35.5		35	37	36.5	330 012.320	0.378	49	50	52.5		50	51	53.5	470 631.626	-0.044
34	36	37.5		35	37	38.5	330 013.230	0.347	49	51	50.5		50	52	51.5	470 635.607	0.153
34	36	36.5		35	37	37.5	330 013.230	0.187	49	51	49.5		50	52	50.5	470 638.541	-0.167
34	36	34.5		35	37	35.5	330 013.230	-0.335	49	51	51.5		50	52	52.5	470 638.541	-0.605
34	36	33.5		35	37	34.5	330 014.649	0.177	49	51	52.5		50	52	53.5	470 640.724	0.414
34	37	39.5		35	38	40.5	330 031.361	-0.254	49	51	48.5		50	52	49.5	470 640.724	0.250
34	37	34.5		35	38	35.5	330 033.067	0.664	49	51	53.5		50	52	54.5	470 640.724	-0.486
34	37	38.5		35	38	39.5	330 033.067	0.342	49	52	49.5		50	53	50.5	470 657.400	0.249
34	37	35.5		35	38	36.5	330 033.067	-0.092	49	52	54.5		50	53	55.5	470 657.400	-0.054
34	37	37.5		35	38	38.5	330 033.067	-0.264	49	52	50.5		50	53	51.5	470 657.400	-0.055
34	37	36.5		35	38	37.5	330 033.067	-0.403	49	52	53.5		50	53	54.5	470 657.400	-0.212
34	31	31.5		35	32	32.5	329 973.435	0.252	49	52	51.5		50	53	52.5	470 657.400	-0.218
34	31	32.5		35	32	33.5	329 973.435	-0.101	49	52	52.5		50	53	53.5	470 657.400	-0.265
34	31	30.5		35	32	31.5	329 973.435	-0.116									
34	31	33.5		35	32	34.5	329 974.821	0.301									
34	31	29.5		35	32	30.5	329 974.821	0.064									
34	31	28.5		35	32	29.5	329 976.800	-0.151									
34	32	34.5		35	33	35.5	329 990.328	0.334									
34	32	33.5		35	33	34.5	329 990.328	0.125									

^aIn MHz.^bNot included in fit.

TABLE II. Selected rotational transitions of Mn^{35}Cl ($v=1,2$) and Mn^{37}Cl ($v=0,1$) ($X^7\Sigma^+$).^a

							Mn^{35}Cl				Mn^{37}Cl			
							$v=1$		$v=2$		$v=0$		$v=1$	
N''	J''	F''	\rightarrow	N'	J'	F'	ν_{obs}	$\nu_{\text{obs}} - \nu_{\text{calc}}$	ν_{obs}	$\nu_{\text{obs}} - \nu_{\text{calc}}$	ν_{obs}	$\nu_{\text{obs}} - \nu_{\text{calc}}$	ν_{obs}	$\nu_{\text{obs}} - \nu_{\text{calc}}$
49	46	47.5		50	47	48.5	468 174.367	0.339	465 759.708	0.188	455 130.850	-0.002	452 828.523	0.124
49	46	46.5		50	47	47.5	468 174.367	0.241	465 759.708	0.132	455 130.850	-0.083	452 828.523	0.041
49	46	48.5		50	47	49.5	468 174.367	0.205	465 759.708	0.004	455 130.850	-0.132	452 828.523	-0.011
49	46	45.5		50	47	46.5	468 174.367	-0.125	465 759.708	-0.197	455 130.850	-0.408	452 828.523	-0.296
49	46	44.5		50	47	45.5	468 174.367	-0.803	465 759.708	-0.842	455 130.850	-1.019	452 828.523	-0.935
49	46	43.5		50	47	44.5	468 176.269	0.049	465 761.726	0.156	455 132.856	0.037	452 830.481	0.023
49	47	49.5		50	48	50.5	468 187.299	1.022	465 772.491	0.889	455 143.569	1.015	452 841.114	0.856
49	47	48.5		50	48	49.5	468 187.299	0.500	465 772.491	0.409	455 143.569	0.552	452 841.114	0.329
49	47	47.5		50	48	48.5	468 187.299	0.024	465 772.491	-0.029	455 143.569	0.113	452 841.114	-0.139
49	47	46.5		50	48	47.5	468 187.299	-0.468	465 772.491	-0.485	455 143.569	-0.349	452 842.417	0.682
49	47	45.5		50	48	46.5	468 188.512	0.140	465 773.470	-0.070	455 144.943	0.456	452 842.417	0.085
49	47	44.5		50	48	45.5	468 188.512	-0.737	465 773.470	-0.902	455 144.943	-0.354	452 842.417	-0.782
49	48	45.5		50	49	46.5	468 197.790	0.156	465 782.969	0.362	455 153.615	0.205	452 851.345	0.037
49	48	46.5		50	49	47.5	468 197.790	-0.513	465 782.969	-0.372	455 154.142	0.097	452 851.345	-0.548
49	48	49.5		50	49	50.5	468 200.591	0.390	465 785.437	0.169	455 156.395	0.655	452 853.860	0.235
49	48	48.5		50	49	49.5	468 200.591	-0.081	465 785.950	0.202	455 156.395	0.161	452 853.860	-0.289
49	48	50.5		50	49	51.5	468 200.591	-0.108	465 785.989	0.111	455 156.395	0.349	452 853.860	0.098
49	48	47.5		50	49	48.5	468 202.640	0.566	465 787.592	0.399	455 158.142	0.607	452 855.737	0.250
49	49	46.5		50	50	47.5	468 202.640	0.117	465 787.592	0.193	455 158.142	-0.129	452 855.737	-0.231
49	49	47.5		50	50	48.5	468 204.968	0.830	465 789.551	0.558	455 160.049	0.217	452 857.651	0.205
49	50	47.5		50	51	48.5	468 204.968	0.776	465 789.551	0.470	455 160.049	-0.130	452 857.651	0.151
49	49	48.5		50	50	49.5	468 204.968	0.068	465 789.551	-0.219	455 161.141	0.582	452 859.070	0.985
49	50	48.5		50	51	49.5	468 204.968	-0.173	465 789.551	-0.526	455 161.141	0.165	452 859.070	0.737
49	49	49.5		50	50	50.5	468 204.968	-0.444	465 789.551	-0.758	455 161.141	0.095	452 859.070	0.591
49	50	49.5		50	51	50.5	468 206.250	0.499	465 791.182	0.460	455 161.141	-0.353	452 859.070	0.217
49	49	50.5		50	50	51.5	468 206.250	0.247	465 791.182	0.249	455 162.166	0.560	452 859.070	0.116
49	50	50.5		50	51	51.5	468 206.250	0.013	465 791.182	-0.051	455 162.166	0.271	452 859.070	-0.204
49	49	51.5		50	50	52.5	468 206.250	-0.258	465 791.182	-0.326	455 162.166	0.116	452 859.070	-0.467
49	50	51.5		50	51	52.5	468 206.250	-0.857	465 791.182	-0.884	455 162.166	-0.490	452 859.805	-0.135
49	50	52.5		50	51	53.5	468 210.139	-0.179	465 795.223	-0.033	455 165.664	-0.145	452 862.983	-0.055
49	51	50.5		50	52	51.5	468 214.007	0.160	465 798.866	0.127	455 169.993	0.056	452 867.071	-0.031
49	51	49.5		50	52	50.5	468 217.022	0.173	465 801.829	-0.002	455 172.429	-0.170	452 869.711	0.013
49	51	51.5		50	52	52.5	468 217.022	-0.530	465 801.829	-0.633	455 172.429	-0.783	452 869.711	-0.573
49	51	48.5		50	52	49.5	468 219.122	0.370	465 804.058	0.351	455 174.533	0.183	452 871.751	0.258
49	51	52.5		50	52	53.5	468 219.122	0.318	465 804.058	0.366	455 174.533	0.233	452 871.751	0.369
49	51	53.5		50	52	54.5	468 219.122	-0.672	465 804.058	-0.601	455 174.533	-0.645	452 871.751	-0.469
49	52	49.5		50	53	50.5	468 235.727	0.548	465 820.484	0.399	455 190.768	0.401	452 887.865	0.463
49	52	50.5		50	53	51.5	468 235.727	0.274	465 820.484	0.133	455 190.768	0.163	452 887.865	0.230
49	52	51.5		50	53	52.5	468 235.727	0.084	465 820.484	-0.038	455 190.768	0.003	452 887.865	0.076
49	52	52.5		50	53	53.5	468 235.727	-0.041	465 820.484	-0.134	455 190.768	-0.095	452 887.865	-0.012
49	52	53.5		50	53	54.5	468 235.727	-0.111	465 820.484	-0.167	455 190.768	-0.137	452 887.865	-0.038
49	52	54.5		50	53	55.5	468 235.727	-0.113	465 820.484	-0.127	455 190.768	-0.111	452 887.865	0.013
50	47	48.5		51	48	49.5	477 473.143	0.264	475 010.254	0.215	464 173.060	0.040	461 824.665	0.158
50	47	47.5		51	48	48.5	477 473.143	0.155	475 010.254	0.147	464 173.060	-0.051	461 824.665	0.065
50	47	49.5		51	48	50.5	477 473.143	0.152	475 010.254	0.053	464 173.060	-0.070	461 824.665	0.043
50	47	46.5		51	48	47.5	477 473.143	-0.209	475 010.254	-0.180	464 173.060	-0.374	461 824.665	-0.271
50	47	45.5		51	48	46.5	477 473.143	-0.871	475 010.254	-0.808	464 173.060	-0.970	461 824.665	-0.893
50	47	44.5		51	48	45.5	477 475.147	0.117	475 012.315	0.269	464 175.003	0.055	461 826.682	0.159
50	48	50.5		51	49	51.5	477 486.002	1.016	475 022.942	0.966	464 185.517	0.934	461 837.107	0.878
50	48	49.5		51	49	50.5	477 486.002	0.492	475 022.942	0.483	464 185.517	0.471	461 837.107	0.351
50	48	48.5		51	49	49.5	477 486.002	0.020	475 022.942	0.048	464 185.517	0.036	461 837.107	-0.112
50	48	47.5		51	49	48.5	477 486.002	-0.456	475 022.942	-0.393	464 185.517	-0.411	461 837.941	0.256
50	48	46.5		51	49	47.5	477 487.222	0.191	475 023.836	-0.031	464 186.392	-0.075	461 837.941	-0.307
50	48	45.5		51	49	46.5	477 487.222	-0.633	475 023.836	-0.810	464 186.392	-0.837	461 837.941	-1.121
50	49	46.5		51	50	47.5	477 496.446	0.204	475 033.441	0.559	464 195.955	0.612	461 847.236	0.064
50	49	47.5		51	50	48.5	477 497.404	0.400	475 033.441	-0.268	464 195.955	-0.109	461 847.236	-0.617
50	49	50.5		51	50	51.5	477 499.252	0.203	475 036.164	0.385	464 198.493	0.596	461 850.083	0.354
50	49	49.5		51	50	50.5	477 499.252	-0.216	475 036.164	-0.045	464 198.493	0.153	461 850.083	-0.124
50	49	51.5		51	50	52.5	477 499.252	-0.434	475 036.603	0.073	464 198.493	0.154	461 850.083	0.103
50	49	48.5		51	50	49.5	477 500.811	-0.035	475 037.594	-0.039	464 199.977	0.361	461 851.463	-0.059
50	50	47.5		51	51	48.5	477 500.811	-0.412	475 037.594	-0.170	464 199.977	-0.319	461 851.463	-0.461
50	50	48.5		51	51	49.5	477 502.705	-0.206	475 039.481	0.051	464 202.222	0.296	461 853.331	-0.143
50	51	48.5		51	52	49.5	477 502.705	-0.336	475 039.481	-0.113	464 202.222	-0.127	461 853.331	-0.273

TABLE II. (*Continued.*)

							Mn^{35}Cl				Mn^{37}Cl			
							$\nu=1$		$\nu=2$		$\nu=0$		$\nu=1$	
N''	J''	F''	\rightarrow	N'	J'	F'	ν_{obs}	$\nu_{\text{obs}} - \nu_{\text{calc}}$	ν_{obs}	$\nu_{\text{obs}} - \nu_{\text{calc}}$	ν_{obs}	$\nu_{\text{obs}} - \nu_{\text{calc}}$	ν_{obs}	$\nu_{\text{obs}} - \nu_{\text{calc}}$
50	50	49.5		51	51	50.5	477 504.377	0.633	475 040.500	0.224	464 203.466	0.747	461 854.714	0.530
50	51	49.5		51	52	50.5	477 504.377	0.354	475 040.500	-0.122	464 203.466	0.292	461 854.714	0.243
50	50	50.5		51	51	51.5	477 504.377	0.050	475 040.500	-0.385	464 203.466	0.194	461 854.714	0.065
50	51	50.5		51	52	51.5	477 504.377	-0.291	475 041.914	0.612	464 203.466	-0.257	461 855.659	0.631
50	50	51.5		51	51	52.5	477 505.629	0.641	475 041.914	0.336	464 204.076	0.178	461 855.659	0.464
50	51	51.5		51	52	52.5	477 505.629	0.440	475 041.914	0.068	464 204.076	-0.079	461 855.659	0.175
50	50	52.5		51	51	53.5	477 505.629	0.142	475 041.914	-0.234	464 204.076	-0.258	461 855.659	-0.116
50	51	52.5		51	52	53.5	477 505.629	-0.531	475 041.914	-0.864	464 204.076	-0.936	461 856.384	0.134
50	51	53.5		51	52	54.5	477 509.205	-0.229	475 045.991	-0.039	464 208.096	-0.128	461 859.295	-0.116
50	52	51.5		51	53	52.5	477 512.717	0.078	475 049.285	0.093	464 212.150	0.101	461 863.324	0.138
50	52	50.5		51	53	51.5	477 515.731	-0.050	475 052.391	-0.038	464 214.750	-0.096	461 865.978	0.082
50	52	52.5		51	53	53.5	477 515.731	-0.829	475 052.391	-0.741	464 214.750	-0.783	461 865.978	-0.576
50	52	49.5		51	53	50.5	477 518.149	0.404	475 054.762	0.395	464 216.892	0.237	461 868.108	0.363
50	52	53.5		51	53	54.5	477 518.149	0.269	475 054.762	0.332	464 216.892	0.208	461 868.108	0.390
50	52	54.5		51	53	55.5	477 518.149	-0.798	475 054.762	-0.709	464 216.892	-0.740	461 868.108	-0.522
50	53	50.5		51	54	51.5	477 534.622	0.460	475 071.119	0.385	464 233.044	0.378	461 884.065	0.422
50	53	51.5		51	54	52.5	477 534.622	0.199	475 071.119	0.132	464 233.044	0.152	461 884.065	0.201
50	53	52.5		51	54	53.5	477 534.622	0.012	475 071.119	-0.035	464 233.044	-0.006	461 884.065	0.050
50	53	53.5		51	54	54.5	477 534.622	-0.125	475 071.119	-0.142	464 233.044	-0.114	461 884.065	-0.049
50	53	54.5		51	54	55.5	477 534.622	-0.220	475 071.119	-0.199	464 233.044	-0.178	461 884.065	-0.099
50	53	55.5		51	54	56.5	477 534.622	-0.263	475 071.119	-0.199	464 233.044	-0.190	461 884.065	-0.086

^aIn MHz.

As a test of the fine and hyperfine assignments, the shift in frequency for each of the 42 hyperfine components relative to the frequency centroid, $\nu_0 = 2B_0N' - 4D_0N'^3$, was evaluated as a function of N' . A plot of this frequency difference, $\nu_{\text{obs}} - \nu_0$, vs N' is displayed in Fig. 2, constructed from the measured frequencies for $\text{Mn}^{35}\text{Cl}(v=0)$, and shown over the entire range of $N' = 15-57$. (There is a discontinuity for one transition that was not measured at $N' = 46$, which is located in a frequency gap of our radiation sources.) Some of these hyperfine components were not resolved at any N and hence trace identical tracks. For the most part, the difference in frequency as a function of N per hyperfine transition follows a smooth curve, suggesting that the assignments are accurate and consistent. There appears to be some oscillation in frequency on the order of a few MHz at intermediate N near the center of the pattern ($\nu_{\text{obs}} - \nu_0 \approx 0$); this effect is a result of line blending, and illustrates the limits of the analysis.

Despite the complexity of the spectra, the final sets of constants obtained in this analysis reproduced the actual data quite well. Representative simulations are shown in Fig. 3. Here the measured spectra of the $N=28 \rightarrow 29$ and $N=47 \rightarrow 48$ transitions at 273.6 and 451.9 GHz are presented in the top panels (left and right). The simulated spectra are shown in the lower panels. The agreement between the real and simulated spectra is quite good, with blended features and relative intensities well reproduced. Fortunately, the actual data had high signal-to-noise ratios, enabling “fine-tuning” of the spectral predictions.

The spectroscopic constants obtained for $\text{Mn}^{35}\text{Cl}(v=0, 1, \text{ and } 2)$ and $\text{Mn}^{37}\text{Cl}(v=0 \text{ and } 1)$ in this analysis are presented in Table III. (Although data for higher vibrational states were observed for Mn^{35}Cl and Mn^{37}Cl , they were not

fit because of their lower signal-to-noise.) The parameters needed for a good fit to the $\text{Mn}^{35}\text{Cl}(v=0)$ data included several higher-order centrifugal distortion corrections to $\lambda(\lambda_D, \lambda_H)$ as well as γ_D , and b_{FD} . Only λ_D and b_{FD} were needed for the other fits. This result is expected, as the $\text{Mn}^{35}\text{Cl}(v=0)$ transitions covered a much wider range of frequency. Inclusion of the higher-order spin terms θ and γ_s did not improve the fit; nor did the use of eQq, the quadrupole coupling constant. However, this result may be a function of the convoluted spectra; the determination of higher-order (and much smaller) parameters is problematic with blended lines. Certainly the rms of the individual fits, which fall in the range 207–256 kHz, are not as small as those usually obtained from millimeter-wave data,¹⁷ but are quite acceptable given the nature of the spectra. Furthermore, the spin and hyperfine parameters determined for both chlorine isotopomers and the vibrationally excited data are consistent with each other, even though they were fit independently. For example, λ lies in the range 1032–1113 MHz for all data sets—a 7% total deviation. The one exception is the dipolar constant c , which is about a factor of three smaller for $\text{Mn}^{35}\text{Cl}(v=0)$ than for the other data fits (32.4 MHz vs 77–114 MHz). Fitting a subset of the data for $\text{Mn}^{35}\text{Cl}(v=0)$ corresponding to the same range of N as for the ^{37}Cl isotopomer and the vibrationally excited states did increase c by 34%—more consistent with the other c constants. Hence, some of the discrepancy in c must be due to the inclusion of lower frequency transitions, where the hyperfine structure was better resolved. The additional difference probably arises from the inherent difficulty in fitting highly blended lines by simulation methods. It should be noted that the 3 σ errors quoted are purely statistical.

The equilibrium spectroscopic constants for Mn^{35}Cl and

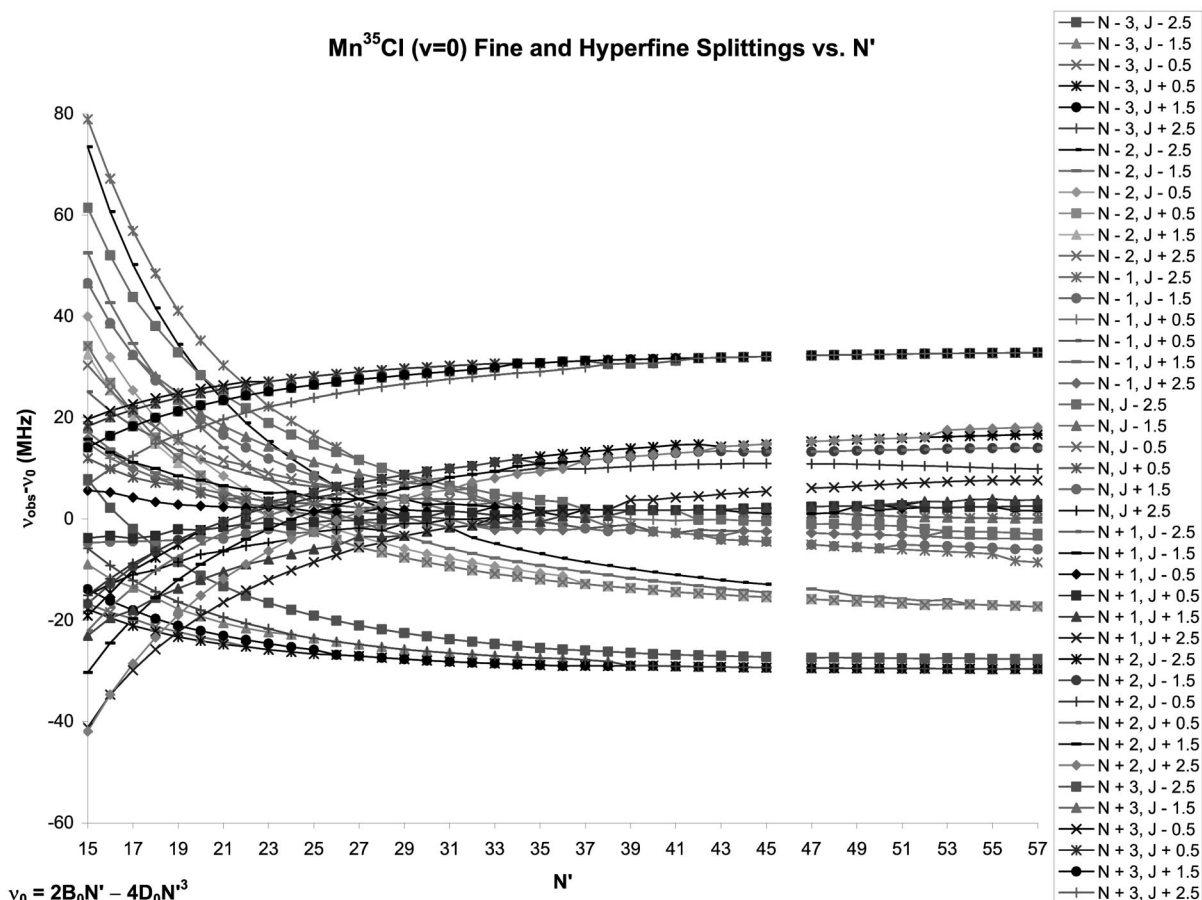


FIG. 2. Graph of the hyperfine splittings of Mn^{35}Cl ($v=0$) as a function of rotational transition. The differences between the measured frequencies, ν_{obs} , of all 42 hyperfine components and the transition centroid, $\nu_0 = 2B_0N' - 4D_0N'^3$, are plotted vs the upper state rotational quantum number, N' . (A single gap arises from a transition that was not measured.) The curves are continuous and lend credence to the spectral assignments. Each fine-hyperfine component is labeled in the legend by its J and F state.

Mn^{37}Cl were calculated as well. B_e and α_e were determined for both isotopomers from their respective rotational constants; these parameters are listed in Table III. The equilibrium bond length r_e of 2.235 Å was also derived. The difference between r_e in Mn^{35}Cl and Mn^{37}Cl is very small (0.000 01 Å), showing that this molecule closely follows the Born–Oppenheimer approximation. The equilibrium vibrational constant was additionally estimated from B_e and D_0 for both isotopomers using $\omega_e \cong (4B_e^3/D_0)^{1/2}$.¹⁸ The determined value for ω_e of 386.30(6) cm^{-1} is very close to that reported by Hayes and Nevin of 380.6 cm^{-1} for the $X^7\Sigma^+$ state of Mn^{35}Cl .¹⁰

V. DISCUSSION

The MnCl radical has a $^7\Sigma^+$ ground state with six unpaired electrons. The electron configuration leading to this ground state is postulated to be

$$X^7\Sigma^+ : (\text{core}) 10\sigma^2 1\delta^2 11\sigma^1 5\pi^2 12\sigma^1. \quad (2)$$

The 10σ orbital forms the bond between the manganese and chlorine atoms. This orbital may be polarized towards the chlorine atom, particularly if MnCl is very ionic. The 1δ , 5π , and 11σ orbitals are nonbonding, as they are mainly $3d$ in

character, and the 12σ orbital is antibonding. The hyperfine parameters determined in this work can be used to test the validity of this electron configuration.

The Fermi contact term b_F in MnCl is relatively large (397.71 MHz for the main isotopomer). As shown in Table IV, it is almost as large as that in MnF (413.6 MHz) and MnO (479.8 MHz). In comparison, the Fermi contact term in Mn^+ (6S) is 698 MHz.¹² Therefore, manganese retains 57% of its original atomic character on formation of MnCl . This result also suggests that manganese chloride, to a large extent, can be described as Mn^+Cl^- .

Only s electrons can contribute to b_F . In MnCl , the $4s$ Mn atomic orbital mixes into the 10σ bonding orbital and 12σ antibonding molecular orbital. The lone 12σ electron, therefore, must be the primary source of the Fermi contact interactions. Another possible contributor is the 11σ orbital. Strictly speaking, it arises from the $d\sigma$ atomic orbital, and therefore, cannot contribute to b_F . However, the 11σ orbital could form with $sd\sigma$ hybridization, and thus contain some $4s$ character, as has been found in MnS .⁵ In fact, this hybridization accounts for the total b_F parameter in manganese sulfide, which is fairly large in magnitude (see Table IV). Furthermore, electrons in a $3d^5$ configuration have angular factors that add to zero [i.e., $2 \times \langle 3 \cos^2 \theta - 1 \rangle_{d^5} + 2$

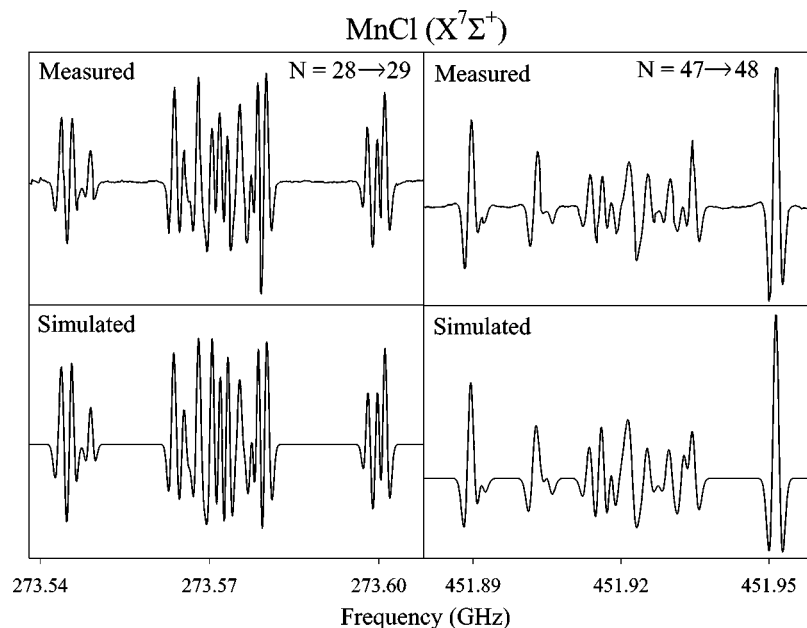


FIG. 3. Comparison of the measured spectra (upper panel) vs the simulated spectra (lower panel) of the $N=28 \rightarrow 29$ and $N=47 \rightarrow 48$ transitions of Mn^{35}Cl ($v=0$) near 273.6 and 451.9 GHz. The simulations agree very well with the recorded spectra, including shoulder features and relative intensities. Each laboratory spectrum is one scan, 70 MHz wide, with an acquisition time of about 1 min.

$\times \langle 3 \cos^2 \theta - 1 \rangle_{d\pi} + \langle 3 \cos^2 \theta - 1 \rangle_{d\sigma} = 2 \times (-\frac{4}{7}) + 2 \times (\frac{2}{7} + \frac{4}{7}) = 0$.⁷ Consequently, a pure $3d^5$ configuration results in a dipolar constant of zero because

$$c = \frac{3}{2} g_e \mu_B g_l \mu_N \sum_i \left\langle \frac{3 \cos^2 \theta - 1}{r_i^3} \right\rangle. \quad (3)$$

If the $3d\sigma$ orbital in this configuration does hybridize with the $4s$ orbital, then the mixing coefficient of the $d\sigma$ electron is less than unity, and the angular factors do not sum to zero. In fact, for MnS and MnO, the $3d\sigma$ contribution is decreased to ~ 0.7 and ~ 0.5 , respectively.^{4,5} The net result is that the c parameter becomes negative in these two species. As shown in Table IV, $c = -27.8$ MHz for MnS and $c = -48.2$ MHz for MnO.

In the case of MnCl (and MnF and MnH), the c parameter is positive, rather than negative. Therefore, $sd\sigma$ hybridization is probably not occurring in these molecules. Instead, the 11σ orbital remains totally $3d$ in character. As a consequence, the $3d$ electrons have their respective angular factors, which add to zero and they, therefore, make no contribution to the c parameter. The remaining orbital in question is the 12σ . As is proposed for MnH,⁷ for better overlap with the Cl $3p$ atomic orbital, the 12σ orbital contains a contribution from the Mn $4p\sigma$ atomic orbital, namely

$$|12\sigma\rangle = c_{4s} | \text{Mn } 4s\sigma \rangle + c_{4p} | \text{Mn } 4p\sigma \rangle + c_{3p} | \text{Cl } 3p\sigma \rangle. \quad (4)$$

If manganese retains 57% of $4s$ character, i.e., $c_{4s}^2 = 0.57$, as

TABLE III. Spectroscopic constants for Mn^{35}Cl and Mn^{37}Cl ($X^7\Sigma^+$).^a

Parameter	Mn^{35}Cl			Mn^{37}Cl	
	$v=0$	$v=1$	$v=2$	$v=0$	$v=1$
B	4722.071 37(18)	4697.8527(30)	4673.7122(30)	4566.3922(16)	4543.3677(30)
D	0.003 164 475(42)	0.003 163 45(57)	0.003 165 24(56)	0.002 959 73(27)	0.002 959 95(56)
γ	11.2658(71)	10.947(15)	10.834(15)	10.649(12)	10.578(17)
γ_D	$-2.73(13) \times 10^{-5}$				
λ	1113.10(72)	1076.9(7.2)	1067.7(6.9)	1031.7(4.1)	1073.2(8.4)
λ_D	$-0.003 255(56)$	$-0.003 491(61)$	$-0.003 659(61)$	$-0.003 681(50)$	$-0.003 381(67)$
λ_H	$-8.9(1.4) \times 10^{-8}$				
b_F	397.71(62)	374.3(4.3)	375.9(4.3)	337.8(2.9)	368.7(4.7)
b_{FD}	$4.87(18) \times 10^{-4}$	$7.53(46) \times 10^{-4}$	$6.50(43) \times 10^{-4}$	$6.44(35) \times 10^{-4}$	$6.46(51) \times 10^{-4}$
c	32.35(99)	94.1(6.6)	77.3(6.5)	94.2(9.3)	114.0(6.6)
rms	0.211	0.243	0.238	0.256	0.207
B_e	4734.148(32)			4577.904(32)	
α_e	24.180(23)			23.024(23)	
r_e (Å)	2.235 151 2(75)			2.235 141 8(78)	
ω_e (cm^{-1})	386.30(6)			379.82(1)	

^aIn MHz, unless otherwise indicated; errors are 3σ in the last quoted digits.

TABLE IV. Comparison of manganese hyperfine parameters.^a

Molecule	Ground state	b_F (MHz)	c (MHz)	Reference
MnH	$7\Sigma^+$	279.1(1.2)	36.0(2.4)	7
MnF	$7\Sigma^+$	413.615(30)	35.584(30)	2
MnCl	$7\Sigma^+$	397.71(62)	32.35(99)	This work
MnO	$6\Sigma^+$	479.86(10)	-48.20(18)	4
MnS	$6\Sigma^+$	206.51(79)	-27.8(1.6)	5

^aFrom millimeter-wave measurements, except for MnH, which used intermodulated fluorescence data; errors are 3σ in the last quoted digits.

comparison with Mn^+ has suggested, then $c_{4p}^2 + c_{3p}^2 = 0.43$. If the chlorine contribution is negligible, as might be indicated by the lack of Cl hyperfine interactions, then $c_{4p}^2 \approx 0.43$. Because the 12σ electron has both s and p character, it is the primary source of both the Fermi contact and dipolar interactions.

The dipolar contribution from the 12σ orbital can be tested by a simple calculation. Assuming that the $4p\sigma$ orbital on manganese is the only source of these interactions, then

$$c = \frac{3}{2} g_e \mu_B g_I \mu_N c_{4p}^2 \left\langle \frac{3 \cos^2 \theta - 1}{r^3} \right\rangle_{4p}, \quad (5)$$

where the angular factor is $4/5$.⁷ Using $c_{4p}^2 = 0.43$ and the radial expectation value for an Mn^+ $4p$ orbital, $\langle r^{-3} \rangle_{4p} = 1.692 \times 10^{25} \text{ cm}^{-3}$,⁷ the calculated value of the dipolar constant is $c = 28.5 \text{ MHz}$ —remarkably close to the measured value of $c = 32.35 \text{ MHz}$. Thus, $sp\sigma$ hybridization of the 12σ orbital is consistent with both hyperfine parameters in MnCl.

Another comparison of interest is the gas-phase versus matrix isolation/ESR hyperfine constants for MnCl. There is fair agreement between these data for the Fermi contact parameter: $b_F(\text{mm-wave}) = 397.71(62) \text{ MHz}$ vs $b_F(\text{ESR}) = 376(11) \text{ MHz}$.¹² For the dipolar term, the ESR value, $c = -102(30) \text{ MHz}$,¹² is larger by a factor of three than the mm-wave value, $c = 32.35(99) \text{ MHz}$, and the sign has changed. The differences are not unexpected because λ and the ESR A parameters are highly correlated. The spin constant was not fit in the matrix analysis, and thus the ESR parameters may be considerably different.

The small value of γ in MnCl (11.3 MHz) relative to the hyperfine parameters is mainly responsible for the highly blended spectra. The magnitude of this constant is determined by the pure microscopic electron spin-nuclear rotation coupling and the second-order spin-orbit effect¹⁹ i.e.,

$$\gamma = \gamma^{\text{sr}} + \gamma^{\text{so}}. \quad (6)$$

The second-order term is predicted to dominate γ in heavier molecules such as MnCl, and arises from perturbations of nearby excited states following the selection rule $\Delta S = 0$.¹⁹ The septet state in MnCl closest in energy to the ground state is the $A^7\Pi$ term. Therefore, the second-order contribution to the spin-rotation interaction for MnCl can be approximated by the expression²⁰

$$\gamma^{\text{so}} = \left(\frac{8}{3} \right)^{1/2} \frac{\langle X^7\Sigma^+ | \text{BL}_- | A^7\Pi \rangle \langle A^7\Pi | \hat{H}_{\text{so}} | X^7\Sigma^+ \rangle}{E(A^7\Pi) - E(X^7\Sigma^+)}. \quad (7)$$

TABLE V. Fine structure parameters of manganese diatomics.^a

Molecule	Ground state	γ (MHz)	λ (MHz)	Reference
MnH	$7\Sigma^+$	939.8(3.2) ^b	-120.5(8.3) ^b	23
MnF	$7\Sigma^+$	16.7152(30)	-136.511(96)	2
MnCl	$7\Sigma^+$	11.2658(71)	1113.10(72)	This work
MnO	$6\Sigma^+$	-70.789(10)	17 198.00(36)	4
MnS	$6\Sigma^+$	-71.800(72)	10 485.0(3.1)	5

^aErrors are 3σ in the last quoted digits; data is for main isotopomer.

^bFourier-transform infrared (FTIR) measurements.

This equation can be simplified assuming that the promotion of the $sp\sigma$ hybridized electron on manganese in the $X^7\Sigma^+$ state to the $4p\pi$ orbital creates the $A^7\Pi$ state. Then the matrix elements do not vanish, and Eq. (7) reduces to

$$\gamma^{\text{so}} = \frac{2}{3} \frac{c_{4p}^2 \langle B \rangle_{\pi\sigma} a_{4p}}{E(A^7\Pi) - E(X^7\Sigma^+)}, \quad (8)$$

where c_{4p}^2 is the mixing coefficient for the $4p$ orbital, as defined in Eq. (4), $\langle B \rangle_{\pi\sigma}$ is the average value of the rotational constants of the $A^7\Pi$ and $X^7\Sigma$ states,⁷ and a_{4p} is the atomic spin-orbit constant of the $4p$ orbital.²¹ Using B_0 for $\langle B \rangle_{\pi\sigma}$, and $6A(A^7\Pi)$ for $a_{4p}[A(A^7\Pi) = 41 \text{ cm}^{-1}]$,^{7,10} $c_{4p}^2 \leq 0.43$, and $27 004.6 \text{ cm}^{-1}$ for $E(A^7\Pi) - E(X^7\Sigma)$,¹⁰ then the second-order term is calculated to be $\gamma^{\text{so}} < 12.3 \text{ MHz}$. Thus it appears that the second-order spin-orbit term is the primary contributor to γ .

The spin-spin parameter for MnCl has a value intermediate between the other manganese-containing molecules, as shown in Table V. However, like MnO and MnS, the sign of λ for MnCl is positive, in contrast to MnH and MnF. The spin-spin parameter λ is the sum of the microscopic electron spin-spin interaction and the second-order spin-orbit coupling arising from excited electronic states, i.e., $\lambda = \lambda^{\text{ss}} + \lambda^{\text{so}}$. The selection rules for the second-order effect are $\Delta S = 0, \pm 1, \Delta \Omega = 0, \Sigma^\pm \leftrightarrow \Sigma^\mp$.¹⁹ Although in general this effect is a summation over many excited states, to a first approximation the main contributor is probably the $A^7\Pi$ state. In this case the spin-orbit interaction can be approximated by the following equation:²⁰

$$\lambda^{\text{so}} = \frac{-30(2S-2)!}{(2S+3)!} \times \sum_{\Sigma} \sum_{\Lambda'\Sigma'} \frac{[3\Sigma^2 - S(S+1)] |\langle A^7\Pi | \hat{H}_{\text{so}} | X^7\Sigma^+ \rangle|^2}{E(A^7\Pi) - E(X^7\Sigma^+)}. \quad (9)$$

This expression has been evaluated by Varberg *et al.*,²² and is equal to

$$\lambda^{\text{so}} = \frac{1}{72} \frac{c_{4p}^2 a_{4p}^2}{E(A^7\Pi) - E(X^7\Sigma^+)}. \quad (10)$$

Assuming the previous values of $c_{4p}^2 = 0.43$, $a_{4p} = 6 \text{ A}$, and the $\Pi - \Sigma$ energy difference, λ^{so} is estimated to be 401 MHz. Therefore, it accounts for $\sim 36\%$ to the total spin-spin constant. This result implies that λ^{ss} is the main contributor to λ . Alternatively, the smaller value of λ^{so} may in part stem

from the assumption of a unique ${}^7\Pi$ perturber. Other excited states such as $(d^5) {}^5\Pi$ may be canceling out the net effect of the $A {}^7\Pi$ state, for example. Further studies of the electronic manifold of MnCl would certainly be useful in resolving this issue.

VI. CONCLUSION

The measurement of the pure rotational spectrum of MnCl has established the rotational parameters for this radical in its $X {}^7\Sigma^+$ ground state for the first time, as well as fine structure and hyperfine constants. Spectral simulation was employed in the analysis and has proven quite useful in the evaluation of the complicated hypermultiplet patterns as observed in MnCl. Second-order spin-orbit effects were estimated to account for only $\sim 36\%$ of the spin-spin constant, but appeared to be the primary contributor to the spin-rotation parameter, considering the nearby $A {}^7\Pi$ state as the perturber. This result suggests that other states may be canceling out the contribution of the $A {}^7\Pi$ state to λ^{so} . While the hyperfine constants in MnCl are similar to those of other manganese-bearing species, their origins vary. In MnCl, as well as MnF and MnH, both the Fermi contact term and the dipolar constant come from the lone electron in the 12σ orbital, which is $sp\sigma$ hybridized. In contrast, the orbitals in MnS and MnO appear to undergo $sd\sigma$ hybridization, which means that the electron in the 11σ (or 9σ) orbital is the primary contributor to c . Although these manganese diatomics appear to be similar species, subtle differences in their bonding are apparent.

ACKNOWLEDGMENTS

This research is supported by NSF Grant Nos. CHE-04-11551 and AST-02-04913. The authors thank Dr. Brian Drouin for the use of his spectral simulation program.

- ¹T. D. Varberg, R. W. Field, and A. J. Merer, *J. Chem. Phys.* **92**, 7123 (1990).
- ²P. M. Sheridan and L. M. Ziurys, *Chem. Phys. Lett.* **380**, 632 (2003).
- ³P. Mesnage, *Ann. Phys. (Paris)* **12**, 5 (1939).
- ⁴K. Namiki and S. Saito, *J. Chem. Phys.* **107**, 8848 (1997).
- ⁵J. M. Thompsen, M. A. Brewster, and L. M. Ziurys, *J. Chem. Phys.* **116**, 10212 (2002).
- ⁶L. Andrews, W. D. Bare, and G. V. Chertihin, *J. Phys. Chem. A* **101**, 8417 (1997).
- ⁷T. D. Varberg, R. W. Field, and A. J. Merer, *J. Chem. Phys.* **95**, 1563 (1991).
- ⁸J. Bacher, *Helv. Phys. Acta* **21**, 379 (1948).
- ⁹W. Hayes, *Proc. Phys. Soc., London, Sect. A* **68**, 1097 (1955).
- ¹⁰W. Hayes and T. E. Nevin, *Proc. R. Ir. Acad., Sect. A* **57**, A2, 15 (1955).
- ¹¹O. Launila, *Mol. Phys.* **76**, 319 (1992).
- ¹²C. A. Baumann, R. J. Van Zee, and W. Weltner, Jr., *J. Phys. Chem.* **86**, 5084 (1982).
- ¹³L. M. Ziurys, W. L. Barclay, Jr., M. A. Anderson, D. A. Fletcher, and J. W. Lamb, *Rev. Sci. Instrum.* **65**, 1517 (1994).
- ¹⁴C. H. Townes and A. L. Schawlow, *Microwave Spectroscopy* (Dover, New York, 1975).
- ¹⁵See EPAPS Document No. E-JCPSA6-121-001448 for a complete list of transitions arising from $Mn^{35}Cl$ and $Mn^{37}Cl$. A direct link to this document may be found in the online article's HTML reference section. The document may also be reached via the EPAPS homepage (<http://www.aip.org/pubservs/epaps.html>) or from <ftp.aip.org> in the directory /epaps/. See the EPAPS homepage for more information.
- ¹⁶H. M. Pickett, *J. Mol. Spectrosc.* **148**, 371 (1991).
- ¹⁷P. M. Sheridan, M. A. Brewster, and L. M. Ziurys, *Astrophys. J.* **576**, 1108 (2002).
- ¹⁸W. Gordy and R. L. Cook, *Microwave Molecular Spectroscopy* (Wiley, New York, 1984).
- ¹⁹H. Lefebvre-Brion and R. W. Field, *Perturbations in the Spectra of Diatomic Molecules* (Academic, Orlando, 1986).
- ²⁰J. M. Brown, E. A. Colbourn, J. K. G. Watson, and F. D. Wayne, *J. Mol. Spectrosc.* **74**, 294 (1979).
- ²¹O. Launila, B. Simard, and A. M. James, *J. Mol. Spectrosc.* **159**, 161 (1993).
- ²²T. D. Varberg, J. A. Gray, R. W. Field, and A. J. Merer, *J. Mol. Spectrosc.* **156**, 296 (1992).
- ²³I. E. Gordon, D. R. T. Appadoo, A. Shayesteh, K. A. Walker, and P. F. Bernath, *J. Mol. Spectrosc.* **229**, 145 (2005).